

# Chapter 6

## Spectral Simulations

In the following sections, the theoretical background and the numerical techniques will be discussed that were employed in the simulation and fitting routines to analyze the spectra presented in chapter 7.

### 6.1 Hamiltonian

The spin Hamiltonian used to describe a paramagnetic radical with an electron spin  $S = \frac{1}{2}$ , coupled to a nucleus with spin  $I$  includes the Zeeman interaction and the hyperfine coupling term:

$$\mathcal{H} = \mathcal{H}_{Ze} + \mathcal{H}_{HFI} = \mu_B \mathbf{B} \cdot \mathbf{g} \cdot \mathbf{S} + \mathbf{S} \cdot \mathbf{A} \cdot \mathbf{I} \quad (6.1)$$

In the Zeeman term  $\mu_B$  is electronic Bohr magneton,  $\mathbf{B}$  is the external magnetic field vector,  $\mathbf{g}$  is the electron  $g$ -tensor,  $\mathbf{S}$  is the electron spin operator. In the hyperfine term,  $\mathbf{A}$  is the hyperfine tensor and  $\mathbf{I}$  is the nuclear spin operator.

Further interactions that are often non-negligible are the nuclear Zeeman and nuclear quadrupole interaction. For the systems and experimental conditions that will be considered below, they can be neglected and therefore are not considered in the current state of the simulation programs.

While they could easily be included without significantly increasing computation time for a single spectrum, they would greatly increase the number of free parameters. When attempting to fit experimental data to a model with an optimization routine this reduces the significance of the other parameters and therefore should be avoided whenever possible.

In all simulation routines, the principal axis system of the  $\mathbf{g}$ -tensor has been chosen as the reference coordinate system. This means that the magnetic field vector  $\mathbf{B}$  and the hyperfine tensor  $\mathbf{A}$  have to be transformed into the  $\mathbf{g}$ -tensor main axis system.

The Zeeman term  $\mathcal{H}_{Zee}$  then takes the form

$$\mathcal{H}_{Zee} = B\mu_B(g_{xx} \cos \phi \sin \theta \mathbf{S}_x + g_{yy} \sin \phi \sin \theta \mathbf{S}_y + g_{zz} \cos \theta \mathbf{S}_z) \quad (6.2)$$

with  $\theta$  and  $\phi$  the angles that determine the orientation of  $\mathbf{B}$  as depicted in Figure 6.1. The hyperfine term  $\mathcal{H}_{HFI}$  becomes

$$\mathcal{H}_{HFI} = \mathbf{S} \cdot \mathbf{A}_g \cdot \mathbf{I} = \mathbf{S} \cdot R(\phi_A \theta_A \psi_A)^{-1} \mathbf{A} R(\phi_A \theta_A \psi_A) \cdot \mathbf{I} \quad (6.3)$$

where  $\mathbf{A}_g$  is the hyperfine tensor in the  $\mathbf{g}$ -tensor main axis system and  $R(\phi_A \theta_A \psi_A)$  is the Euler rotation matrix as defined in (H. Goldstein 1951), which rotates the hyperfine tensor main axis system into the  $\mathbf{g}$ -tensor main axis system.

## 6.2 Calculating Transitions

To calculate the spectral transitions, two different routes can be taken. One is to set up the Hamiltonian, perform a numerical diagonalization and then determine the transition probabilities between the states. The second is to analytically calculate the resonance positions via perturbation theory. Both approaches have been employed here.

While the perturbation solution has the advantage of being faster, the diagonalization approach has the advantage of being inherently exact and

to lend itself easily to an extension to include further interactions in the Hamiltonian. Since the time-consuming step in the diagonalization routine is the actual diagonalization of the Hamiltonian matrix itself, including further Hamiltonian terms will not increase computation times as long as the matrix dimensions remain the same.

### 6.2.1 Numerical Diagonalization

To obtain the field values for the allowed transitions, the Hamiltonian matrix was constructed from the basic spin matrices. The dimension of the Hamiltonian matrix is then  $(2S+1)(2I+1)$  with  $S = \frac{1}{2}$  and  $I = 0, \frac{1}{2}, 1$  the electron and nuclear spin quantum numbers considered.

Subsequently, eigenvalues and eigenstates were obtained via direct numerical diagonalization (The Mathworks, Inc. 1999).

### 6.2.2 Transition Probability

To derive an expression for the transition probability  $P_{ij}$  between two energy levels  $E_i$  and  $E_j$ , I want to follow the treatment of (G. van Veen 1978).

Microwave absorption is possible when the energy separation of two levels becomes approximately equal to the energy quantum of the radiation:

$$\Delta_{ij} = |E_i(\mathbf{B}) - E_j(\mathbf{B})| \approx \hbar\omega \quad (6.4)$$

In an excitation microwave field of the form  $\mathbf{B}_1 \exp(i\omega t)$ , where  $B_1$  is the magnetic field amplitude of the radiation, the transition probability can be written as:

$$P_{ij}(\mathbf{B}, \mathbf{B}_1) = M_{ij}(\mathbf{B}, \mathbf{B}_1) f(\Delta_{ij}(\mathbf{B}) - \hbar\omega) \quad (6.5)$$

with

$$M_{ij}(\mathbf{B}, \mathbf{B}_1) = |\langle i | \mathcal{H}_1(\mathbf{B}_1) | j \rangle|^2 \quad (6.6)$$

Here  $\mathcal{H}_1 \exp(i\omega t)$  is the time-dependent Hamiltonian perturbing the system and  $f(\Delta_{ij}(\mathbf{B}) - \hbar\omega)$  is the lineshape function.

Only the usual experimental setup with  $\mathbf{B}_1$  perpendicular to  $\mathbf{B}$  will be considered. The main reference coordinate system is the main axis system of the  $\mathbf{g}$  tensor, the direction of the external field  $\mathbf{B}$  can then be described by the two Euler angles  $\theta$  and  $\phi$ . The third angle  $\chi$  describes the orientation of  $\mathbf{B}_1$  as shown in Figure 6.1:

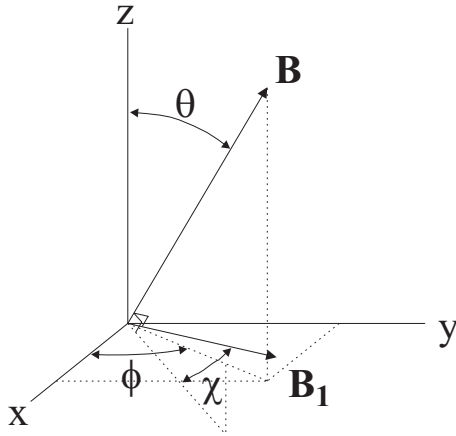


Figure 6.1: Euler angles used to describe the orientation of the external magnetic field  $\mathbf{B}$  and the excitation microwave field  $\mathbf{B}_1$  with respect to the  $\mathbf{g}$  tensor main axis system. Right angles are marked with a square between the respective vectors.

For a particular orientation of the external magnetic field the transition probability still depends on the orientation of  $\mathbf{B}_1$ . To calculate a powder spectrum only the average over all angles  $\chi$  is needed:

$$\langle M_{ij} \rangle = \int_0^\pi d\chi |\langle i | \mathcal{H}_1(\mathbf{B}_1) | j \rangle|^2 \quad (6.7)$$

Writing  $\mathbf{B}$  and  $\mathbf{B}_1$  in terms of the Euler angles  $\theta$ ,  $\phi$  and  $\chi$  as in Figure 6.1

$$\mathbf{B} = B(\sin \theta \cos \phi; \sin \theta \sin \phi; \cos \theta)$$

$$\mathbf{B}_1 = B(\cos \theta \cos \phi \cos \chi - \sin \phi \sin \chi; \cos \theta \sin \phi \cos \chi + \cos \phi \sin \chi; -\sin \theta \cos \chi)$$

and using

$$\int_0^{\pi} \cos^2 \chi d\chi = \int_0^{\pi} \sin^2 \chi d\chi = \frac{\pi}{2}$$

$$\int_0^{\pi} \cos \chi \sin \chi d\chi = 0$$

one obtains for the transition probability  $\langle M_{ij} \rangle$ :

$$\begin{aligned} \langle M_{ij} \rangle = & (1 - \sin^2 \theta \cos^2 \phi) S_{x_{ij}}^* S_{x_{ij}} \\ & - \sin^2 \theta \sin \phi \cos \phi [S_{x_{ij}}^* S_{y_{ij}} + S_{y_{ij}}^* S_{x_{ij}}] \\ & - \cos \theta \sin \theta \cos \phi [S_{x_{ij}}^* S_{z_{ij}} + S_{z_{ij}}^* S_{x_{ij}}] \\ & + (1 - \sin^2 \theta \sin^2 \phi) S_{y_{ij}}^* S_{y_{ij}} \\ & - \cos \theta \sin \theta \sin \phi [S_{y_{ij}}^* S_{z_{ij}} + S_{z_{ij}}^* S_{y_{ij}}] \\ & + \sin^2 \theta S_{z_{ij}}^* S_{z_{ij}} \end{aligned} \quad (6.8)$$

Here  $S_{k_{ij}} = \langle V_i | S_k | V_j \rangle$ , where  $V_i$  and  $V_j$  are the Eigenvectors corresponding to energy levels  $i$  and  $j$  and  $k = x, y, z$ .

Since the Matlab routine used for diagonalization of the Hamiltonian readily computes all Eigenvectors together with the diagonalized matrix, the above expression can directly be evaluated.

### 6.2.3 Perturbation Solution

The expressions for the resonance field values for a Hamiltonian as in equation 6.1 can be obtained from the literature. Following (N. M. Atherton 1993), under neglect of the nuclear Zeeman interaction and treating the hyperfine interaction to first order, for the  $\Delta M_S = 1$ ,  $\Delta M_I = 0$  transitions one obtains an energy difference of

$$\Delta E = g_{eff} \mu_B B + M_I \frac{1}{g_{eff}} \sqrt{\mathbf{1} \cdot \mathbf{g} \cdot \mathbf{A} \cdot \mathbf{A} \cdot \mathbf{g} \cdot \mathbf{1}} \quad (6.9)$$

with the orientation-dependent effective  $g$ -value  $g_{eff}(\theta, \phi)$

$$\begin{aligned} g_{eff} &= \sqrt{\mathbf{l} \cdot \mathbf{g} \cdot \mathbf{g} \cdot \mathbf{l}} \\ &= \sqrt{g_{xx}^2 \cos^2 \phi \sin^2 \theta + g_{yy}^2 \sin^2 \phi \sin^2 \theta + g_{zz}^2 \cos^2 \theta} \end{aligned} \quad (6.10)$$

and the unit vector in direction of the magnetic field:

$$\mathbf{l} = (\cos \phi \sin \theta; \sin \phi \sin \theta; \cos \theta) \quad (6.11)$$

Solving equation 6.9 for  $B$ , the resonance fields for each value of  $M_I$  can be calculated.

Both approximations, the neglect of the nuclear Zeeman interaction and developing the Hamiltonian to first order only are usually good approximations in the limit of high external magnetic fields  $B_0$ .

### 6.3 Powder Averages

In order to simulate EPR spectra of radicals in frozen solution or in powders, one has to take into account all possible molecular orientations. In principle it is possible that certain orientations are favored to others to yield an anisotropic orientation distribution. This is often the case for thin films adsorbed onto plane surfaces or samples using liquid crystals as solvent. The samples investigated in the present work however could all be successfully simulated assuming a completely isotropic orientation distribution.

The most straightforward way to generate the powder orientations is to loop over the polar and azimuthal angles  $\theta$  and  $\phi$  in equal step sizes and then correct for the uneven distribution of evaluated orientations per solid angle with a correction factor of  $\sin \theta$ . Using this approach, to generate a sufficiently high density of orientations on the unit sphere for a certain precision one has to sample excessive points in the polar region around the  $z$ -axis.

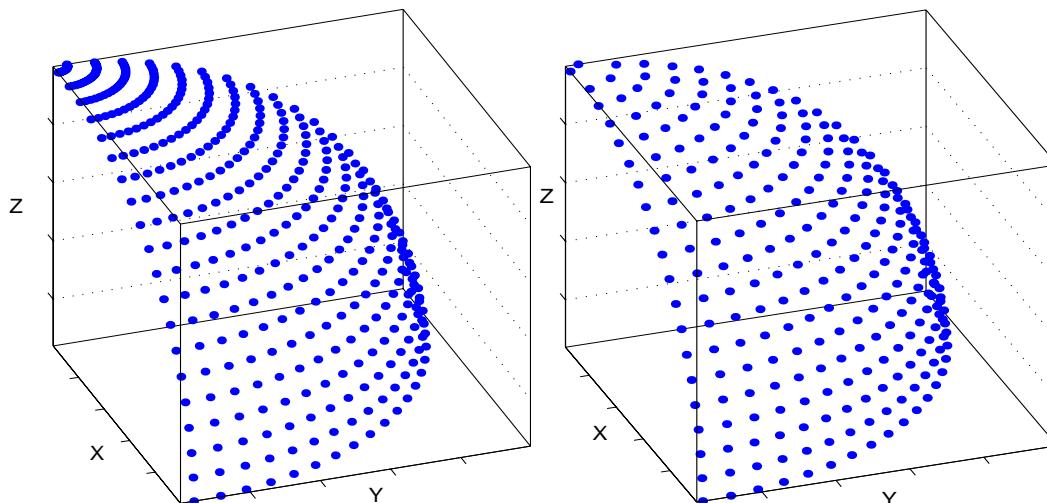


Figure 6.2: Comparison of the orientations evaluated by the “standard” powder generation algorithm (left) and by the “igloo”-algorithm (right).

To avoid this, in this work a different orientation selection scheme has been chosen. In this scheme, commonly dubbed the “igloo-method” (M. J. Nilges 1979), the unit sphere is divided into regions of equal solid angles (the “bricks”) and the sample point chosen exactly in the center of each region. Thus the distribution of sample orientations is completely uniform and no excess orientations have to be evaluated.

The difference between the two approaches becomes obvious in the renderings in figure 6.2. Both sets of points were generated with 20  $\theta$ -steps in the first octant. While both sets provide the same minimum precision, the standard algorithm has to evaluate 400 orientations and the igloo method only 264. Depending on the relative orientation of the involved tensors, an integration over more than one octant may have to be performed.

In the simple version of the igloo-method, a step width for the polar angle  $\theta$  is chosen first, then for each value of  $\theta$  a step width for the azimuthal angle  $\phi$  is calculated to yield the same arc on a parallel of latitude. This approach leads to a round-off error, since the igloo bricks usually do not exactly close

off the unit sphere at the edges. This roundoff-error approaches zero for small step widths, of course.

In the powder-scheme used here, the roundoff-error is avoided. In a first loop, the number of bricks which would be used by the conventional igloo-method is calculated. Then the area occupied by one brick on the surface of the unit sphere is calculated. In a second loop, the step widths for  $\theta$  and  $\phi$  are then adjusted such that each layer exactly closes off at the edge. The orientations where the Hamiltonian is evaluated are chosen at the center of each brick.

Compared to the conventional igloo-method, which basically is an “equal step size method”, the approach used here could be called “equal solid angle method”.

A further significant improvement in the calculation time of powder spectra can be achieved by employing schemes that allow for interpolation. Here, the points where the function is evaluated lie on an easy to parameterize line and additional function values can be obtained by interpolating between the actually evaluated ones. Two examples employing this technique are the so-called SOPHE method (Wang & Hanson 1995) and the interpolation scheme by Alderman et al. (Alderman et al. 1986)

Since there is no way to easily parameterize the positions of the evaluation points of the igloo-methods, an interpolation scheme cannot be introduced here. To further speed up calculations, the implementation of the Alderman-algorithm is planned for a coming version of the simulation routines.

## 6.4 Orientation-dependent Linewidths

An effect that becomes more pronounced at higher magnetic fields is a dependency of the linewidth  $\Gamma$  of the spectral transitions on the orientation of the molecules with respect to the magnetic field. The actual effects underlying



this behavior are discussed in subsection 7.2.1.

To account for this in the simulations, orientation–dependent linewidths  $\Gamma_k(k = x, y, z)$  were introduced into the formalism. This of course is a purely empirical approach. For the case of the anisotropic broadening of the lines being due to a distribution of environment effects such as solvent polarity, an empirical approach can be justified. Under certain conditions for the distribution function, it enables one to use a least squares minimization routine to extract the remaining parameters of the Hamiltonian such as (average)  $g$ –values and hyperfine constants.

The linewidths were taken to lie on an ellipsoid fixed to the molecular frame, colinear with the  $g$ –tensor. The main values of the ellipsoid then are the linewidths in  $x$ ,  $y$  and  $z$ –direction, respectively. To obtain the linewidth for an arbitrary orientation with polar angle  $\theta$  and azimuthal angle  $\phi$  we need the equation for the ellipsoid:

$$\frac{x^2}{\Gamma_x^2} + \frac{y^2}{\Gamma_y^2} + \frac{z^2}{\Gamma_z^2} = 1$$

and  $x$ ,  $y$  and  $z$  in spherical coordinates:

$$x = R \sin \theta \cos \phi, y = R \sin \theta \sin \phi, z = R \cos \theta$$

Taking the effective linewidth  $\Gamma_{eff}$  for the distance to the ellipsoid surface  $R$  for a given orientation with polar angles  $\theta$  and  $\phi$  we can solve for  $\Gamma_{eff}$ :

$$\Gamma_{eff} = \left[ \frac{\sin^2 \theta \cos^2 \phi}{\Gamma_x^2} + \frac{\sin^2 \theta \sin^2 \phi}{\Gamma_y^2} + \frac{\cos^2 \theta}{\Gamma_z^2} \right]^{-\frac{1}{2}} \quad (6.12)$$

The inclusion of orientation–dependent linewidths unfortunately prevents the use of some time–saving routines when convoluting the stick pattern with a lineshape. In particular it is not possible to perform a convolution via a multiplication in Fourier space or to evaluate the line shape once and then perform a look–up. In the present routine, immediately after evaluating the transition field positions for a certain orientation, a single line is added to

the sum spectrum. Currently this step is the most time-consuming part of the algorithm.